PCCP

Accepted Manuscript

ROYAL SOCIETY OF CHEMISTRY

www.rsc.org/pccp

Cite this: DOI:

www.rsc.org/xxxxxx

Paper

Thermodynamic Stability and Structure of Cuprous Chloride Surfaces: A Density Functional Theory Investigation

Ibrahim A. Suleiman [*a], Marian W. Radny[b, †], Michael J. Gladys[b], Phillip V. Smith[b], John C. Mackie[c ††], Eric M. Kennedy[c] and Bogdan Z. Dlugogorski[d]

Received (in XXX, XXX) Xth XXXXXXXXX 20XX, Accepted Xth XXXXXXXXX 20XX
DOI: 10.1039/b000000x

Density functional theory together with *ab initio* atomistic thermodynamics has been utilized to study the structures and stabilities of the low index CuCl surfaces. It is shown that the Cl-terminated structures are more stable than the Cu-terminated configurations, and that the defected CuCl(110)-Cu structure is more stable than the stoichiometric CuCl(110) surface. The equilibrium shape of a cuprous chloride nanostructure terminated by low-index CuCl surfaces has also been predicted using a Wulff construction. It was found that the (110) facets dominate at low chlorine concentration. As the chlorine concentration is increased, however, the contributions of the (100) and (111) facets to the Wulff construction also increase giving the crystal a semi-prism shape. At high chlorine concentration, and close to the rich limit, the (111) facets were found to be the only contributors to the Wulff construction, resulting in prismatic nano-crystals.

1. Introduction

Recently, there has been considerable interest in studying the effect of the shapes and facets of crystallite catalysts on their reactivity and selectivity in chemical reactions. Many studies have shown that the specific exposed crystal plane plays an important role in the reactivity of the catalyst, due mainly to the diverse arrangements of the surface atoms and number of dangling bonds on different crystal planes [1, 2]. In reality, catalysts are usually composed of many crystals with a variety of crystal planes where the reactions usually take place. This makes the activity of a catalyst lower than a shape-controlled crystallite.

The shape of a crystal can be controlled by varying the temperature, pressure and concentration of the components in the surrounding environment [1, 3-13]. In this paper we study theoretically the structure and stability of different CuCl surfaces over a wide range of temperatures and pressures. This has been done by extrapolating the results of density functional theory (DFT) calculations performed at T = 0 K and p = 0 atm, to the experimental T and p conditions using the methodology of *ab initio* atomistic thermodynamics. Such an investigation is important for many technologically important processes where CuCl is involved as a catalyst, such as free radical polymerization and HCl oxidation [14, 15].

The growth of CuCl crystal has been investigated for both environmental and catalytic purposes. Nakakura *et al.* [16, 17] reported the formation of CuCl clusters with (111) facets when they studied chlorine adsorption on the Cu(100) surface under Ultra High Vacuum (UHV) conditions. The formation of the CuCl phase with a Cl-terminated (111) plane at high pressure and low temperatures has also been reported by Galeotti *et al.*.[18] Wang *et al.* [19] have investigated the formation and morphology of CuCl crystals on bronze surfaces using X-ray diffraction (XRD) and atomic force microscopy (AFM). They have observed triangular shaped crystals revealing the typical characteristics of the CuCl (111) crystal group. Their XRD measurements also

detected the (110) crystal plane; however, the (111) crystal face was predominant. Tomizuka *et al.* [11], at temperature of 373-570 K and atmospheric pressure, found in their morphology study of CuCl crystal growth from Cu-halide vapour that the CuCl crystals that were grown on the quartz tube formed the (111) polar surface. Recently, Xie *et al.* [1] investigated the effect of the CuCl crystal shape on the reactivity and selectivity of the crystal by synthesising CuCl crystallites with step-morphologies including tetrahedral, face-centered-etched tetrahedral, tripod dendrites and tetrapods. They found that under atmospheric pressure and maximum temperature of 415 K, the powder XRD data for different morphologies consist mainly of (111) and (110) facets with different ratios depending on the shape of the crystal. However, those with more (111) facets exhibited greater reactivity.

In this paper we present the geometries and stabilities of various terminations of low-index CuCl surfaces. We show that, in general, Cl-terminated structures are more favourable than Cu-terminated configurations. We also present the Wulff construction of cuprous chloride in a chlorine environment. We illustrate that while the (110) facet dominates at the chlorine-lean limit, the (111) facet dominates at high chlorine concentration giving the crystal a prismatic shape.

2. Methodology

2.1. Density functional theory: Basis set and convergence

The total energies of slabs representing different surface structures as well as the bulk and molecular reference energies were obtained within the framework of density functional theory (DFT) using the DMol^3 code [20, 21]. The generalized gradient approximation (GGA) of Perdew and Wang [22, 23] was employed to include the exchange-correlation effects. The double numeric basis set with polarization functions (DNP) was used to expand the wave function with a Fermi smearing of 0.136 eV and a real space cutoff of 4.4 Å. Spin polarization was included to allow for electronic spin relaxation.

Symmetric slabs (with inversion symmetry) of (2×2) supercells with 17-19 layers and a 30 Å vacuum region between adjacent slabs have been used to simulate the various CuCl surfaces. The Brillouin zone integrations have been performed using the 12×12×1 Monkhorst-Pack **k**-point sampling set [24] for all surfaces. For all slabs the three center layers were fixed at bulk values while the rest of the atoms were allowed to relax. The tolerances on the energy, gradient, and displacement convergence were set to 2×10^{-6} eV, 5×10^{-4} eV/Å, and 5×10^{-3} Å, respectively.

The shapes of the CuCl crystal at thermal equilibrium corresponding to different chlorine chemical potentials were obtained by the Wulff construction [25]. The Wulff construction predicts an optimal crystal shape that minimizes the surface free energy. The program WinXMorph was used to plot the crystal morphology [26, 27], where the distance of each facet from the center of the crystal was determined by the facet surface free energy.

2.2. Ab initio atomistic thermodynamics

The outputs of the DFT calculations described above are used as inputs to atomistic thermodynamics calculations in order to investigate the relative thermodynamic stability of different CuCl surfaces. In a multi-component system, the gaseous environment acts as a reservoir that can give (or take) atoms to (or from) the surface. When the surface is in equilibrium with the gaseous

reservoir, the most stable surface structure is the one that minimizes the surface free energy, γ, at constant T and p. Following the approach adopted by Reuter and Scheffler [28, 29], the surface free energy for a system of a CuCl surface in a chlorine environment can be described as

$$\gamma(T,p) = \frac{1}{A}\Big[G^{Slab}(T,p,N_{Cl},N_{Cu}) - N_{Cu}g^{bulk}_{CuCl}(T,p) - \frac{1}{2}(N_{Cl}-N_{Cu})E_{Cl_2} - (N_{Cl}-N_{Cu})\Delta\mu_{Cl}(T,p)\Big] \quad (1)$$

where G^{Slab} is the Gibbs free energy of the slab, N_{Cu} and N_{Cl} are the number of atoms of Cu and Cl, respectively, A is the slab surface area, g^{bulk}_{CuCl} is the Gibbs free energy of bulk CuCl, E_{Cl_2} is the energy of an isolated chlorine molecule and $\Delta\mu_{Cl}$ is the relative chlorine chemical potential ($\Delta\mu_{Cl} = \mu_{Cl} - \frac{1}{2}E_{Cl_2}$). Previous works[28-33] have shown that the Gibbs free energy term can be approximated by the DFT calculated total energy of the slab (i.e. G^{slab}=E^{slab}).

Mathematically, $\Delta\mu_{Cl}$ can range from $-\infty$ to $+\infty$. However, the physically meaningful range for $\Delta\mu_{Cl}$ has to have lower and upper bounds. A reasonable estimates of the chlorine chemical potential limits at equilibrium, and T = 0 K and p = 0 atm, are given by

$$\Delta G^{f}_{CuCl}(0,0) < \Delta\mu_{Cl}(T,p) < 0 \quad (2)$$

where $\Delta G^{f}_{CuCl}(0,0)$ is the heat of formation of bulk copper chloride at 0 K and 0 atm. Substituting the upper and lower limits from Eq. (2) into Eq. (1), the chlorine-poor and chlorine-rich limits become:

$$\gamma^{Cl-poor} = \frac{1}{A}[G^{Slab} - N_{Cu}g^{bulk}_{CuCl} - (N_{Cl}-N_{Cu})(g^{bulk}_{CuCl} - g^{bulk}_{Cu})] \quad (3)$$

and

$$\gamma^{Cl-rich} = \gamma^{Cl-poor} + \frac{1}{A}\Big[\big((N_{Cl}-N_{Cu})\Delta G^{f}_{CuCl}\big)\Big] \quad (4)$$

It can be seen from Eq. (3) that atomic or molecular quantities do not enter into the calculation of the chlorine-poor limit at all. This limit thus provides a reliable reference involving only bulk or slab quantities[28-31].

The dependence of γ on temperature T and pressure p comes from the assumption that the surrounding Cl_2 atmosphere acts as an ideal gas reservoir. The required T and p dependence thus arises from the expression

$$\Delta\mu_{Cl}(T,p) = \mu_{Cl}(T,p^\circ) + \frac{1}{2}kTln\left(\frac{p_{Cl_2}}{p^\circ}\right) \quad (5)$$

where k is the Boltzmann constant, p^o is the atmospheric pressure, and the values of $\mu_{Cl}(T,p^\circ)$. The latter includes the contributions from the rotations and vibrations of the Cl_2 molecule as well as the ideal-gas entropy at 1 atm and can be obtained from

$$\mu_{Cl}(T,p^\circ) = \frac{1}{2}[H(T,p^\circ,Cl_2) - H(0\,K,p^\circ,Cl_2)] - \frac{T}{2}[S(T,p^\circ,Cl_2) - S(0\,K,p^\circ,Cl_2)] \quad (6)$$

where H and S are the enthalpy and entropy, respectively. Values for H and S under atmospheric pressure conditions can be found in thermodynamic tables [32]. Some values of $\mu_{Cl}(T,p^\circ)$ for temperatures of interest are shown in Table 1.

Table 1: $\mu_{Cl}(T,p^\circ)$ in the temperature range of interest in our study calculated using Eq. (6).

T (K)	300	400	500	600	700
$\mu_{Cl}(T,p^\circ)$ (eV)	-0.29	-0.42	-0.54	-0.67	-0.80

3. Results and Discussion

3.1. Bulk CuCl

At ambient conditions CuCl crystallizes in the zinc-blende structure with space group $F\bar{4}3M$. In the conventional FCC unit cell, a Cu atom is located at (0, 0, 0) and a Cl atom at (1/4, 1/4, 1/4). Each Cl (Cu) atom thus has four Cu (Cl) nearest neighbours in a tetrahedral configuration (see Figure 1).

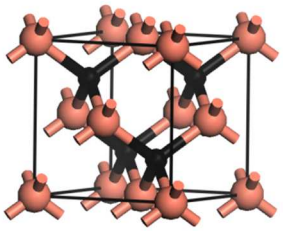

Figure 1: (Colored online) Crystal structure of cuprous chloride (CuCl). In this figure and subsequent figures, the pink (generally larger) circles denote the copper atoms and the black (generally smaller) circles represent the chlorine atoms.

A Monkhorst-Pack [24] 8×8×8 **k**-point sampling set has been used to optimize the CuCl bulk crystal. Our calculated CuCl lattice constant of 5.50 Å is in good agreement with the experimental (5.42 Å) [33] and theoretical (5.47 Å) values [3, 30]. Our calculated heat of formation (-1.15 eV) is seen to underestimate the experimental value (-1.42 eV) [33] by approximately 20%. This is in better agreement with experiment than previous work [30] where the difference was 31%. For consistency within the overall methodology, we have used the computed value (rather than the experimental value) to determine the lower limit of the quantity $\Delta\mu_{Cl}(T, p^{\circ})$.

3.2. The low index surfaces

In this study we have investigated the three low index (100), (110), and (111) surfaces of the CuCl crystal. The ideal (100) and (111) surfaces form polar surfaces with two possible terminations, either Cu or Cl. The (110) surface has been found to be the only stoichiometric structure among all those investigated. The terminology CuCl(*hkl*):L has been used to identify the structure, where *hkl* and L refer to the surface plane and termination, respectively. The ideal low index surfaces are shown in Figure 2. Since surface reconstruction could considerably lower the surface free energy of any of the CuCl surfaces, and significantly influence the overall shape of the Wulff construction, we have also investigated defected surfaces obtained by removing from the ideal (2×2) structures a single copper or chlorine atom. The notation CuCl(*hkl*):L–B has been used to express this action where –B indicates removing a B element atom from the surface.

3.2.1. The CuCl(100) surface

Both the Cu-terminated [CuCl(100):Cu] and Cl-terminated [CuCl(100):Cl] surfaces have been considered for the ideal CuCl(100) surface, as well as defected structures. The investigated CuCl(100) structures are listed in Table 2.

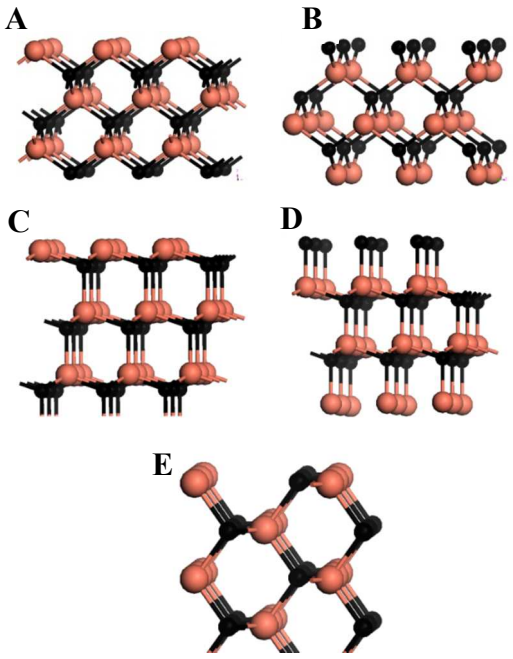

Figure 2: (Colored online) Side views of the ideal CuCl surface structures. (A) CuCl(100):Cu, (B) CuCl(100):Cl, (C) CuCl(111):Cu, (D) CuCl(111):Cl, and (E) the stoichiometric CuCl(110) surface.

The Cl-terminated surface exhibits only small relaxation with shortening of the Cu-Cl bond length at the surface and elongation of the Cu-Cl bond between the second and third layers. The Cu-Cl bond length at the surface of 2.23 Å was found to be 6% shorter than the bulk value (2.381 Å), while almost 7% elongation was determined for the bond length (2.54 Å) between the second and third layers (see Figure 4, B). Similar trends have

been obtained for the Cu-terminated surface (see Figure 4, A) with the Cu-Cl bond length at the surface (2.31 Å) being 3% shorter than the bulk value, whereas 1% elongation has been predicted for the Cu-Cl bond length (2.41 Å) between the second and third layer.

Table 2 shows the calculated surface free energies at the boundaries (i.e. Cl-lean and Cl-rich). The surface free energies of the different CuCl(100) structures are plotted in Figure 3 as a function of chlorine chemical potential as well as T and p. For each structure, the total variation of the surface free energy can be determined from its values at the Cl-lean and Cl-rich limits. The lines connecting these limits are a consequence of the first order relation represented by Eq. (1). The obtained results demonstrate that the chlorine terminated slabs show a negative slope, while the Cu-terminated surfaces show a positive slope. This indicates that the Cl-terminated structures are more favourable in a chlorine–rich gaseous environment, while the Cu-terminated configurations are more favourable at Cl-lean limit. However, Figure 3 also illustrates that two surface structures - CuCl(100):Cl and CuCl(100):Cl-Cu - exhibit the lowest surface free energies among all calculated CuCl(100) configurations (see also Table 2).

Figure 3 elucidates that the CuCl(100):Cl surface is the most stable configuration in the range $-1.15 < \Delta\mu_{Cl} < -0.23$ eV, while close to the Cl-rich limit the CuCl(100):Cl-Cu defected structure is marginally more favourable. Figure 3 also shows that the production of the latter structure is associated with high pressure values - at T= 300 K, CuCl(100):Cl-Cu is predicted to be produced at p~10^3 atm, while at T = 400 K this structure is expected to be produced at p~10^4 atm. However, beyond p~10^4 atm our predictions are not reliable due to the phase transition in the CuCl crystal structure (see discussion in section 3.3).

Table 2: Surface free energies in meV/Å^2 for the (2×2) CuCl(100) structures.

Structure	γ^{lean}	γ^{rich}
CuCl(100):Cu	113.1	151.1
CuCl(100):Cu-Cu	15.4	34.4
CuCl(100):Cu-Cl	41.2	98.1
CuCl(100):Cl	-1.4	-39.4
CuCl(100):Cl-Cl	3.0	-16.1
CuCl(100):Cl-Cu	14.2	-42.7

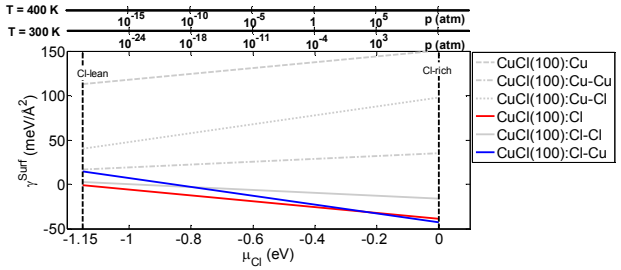

Figure 3: (Colored online) Surface free energy of the CuCl(100) surface structures listed in Table 2. The dotted vertical lines indicate the allowed range for $\Delta\mu_{Cl}$.

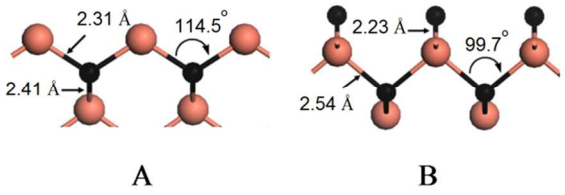

Figure 4: (Colored online) Geometries of the optimized structures of (A) CuCl(100):Cu and (B) CuCl(100):Cl.

3.2.2. The CuCl(110) surface

The ideal CuCl(110) surface is the only stoichiometric structure that we have investigated with the number of chlorine atoms being equal to the number of copper atoms. In addition to the ideal structure, we have calculated the energies for the defected structures obtained by removing Cl or Cu atoms from the surface (see Table 3). Our predicted reconstruction of the ideal CuCl(110) surface is in agreement with the observations of Duke *et al.* [34], and Tsai *et al.* [35, 36]. Calculated values for the parameters characterising this reconstructed surface (see Figure 5) are given in Table 4. The surface was found to exhibit a bond rotation of 26.2º, consistent with the reported semi-empirical value of 29º±3º [34]. We have also observed a 0.04 Å contraction in the bond

length at the top layer. Surface free energy values for the CuCl(110) surface structures are listed in Table 3 and plotted as a function of the chlorine chemical potential as well as T and p in Figure 6. These results show that the defected CuCl(110)-Cu structure is the most stable configuration over the entire range of $\Delta\mu_{Cl}$, rather than the stoichiometric surface [CuCl(110)]. Our result is consistent with the findings of Soon et al [37] who showed that the defected Cu_2O surfaces, which form polar configurations, are more stable than the Cu_2O stoichiometric structures. This result could be important for certain catalytic reaction. Figure 6 shows that there is no other structure that can compete with the CuCl(110)-Cu configuration for any values of the applied T and p. It should be noted, however, that beyond the values p~10^4 atm and T = 700 K result unreliable predictions due to the phase transition to the CuCl crystal structure (see discussion in section 3.3).

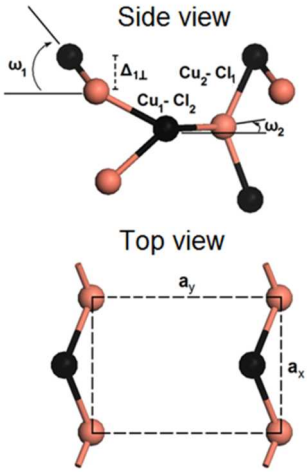

Figure 5: (Colored online) Side and top views of the reconstructed CuCl(110) surface showing the traditional structural variables used to describe zinc-blende (110) surfaces. The unrelaxed structure is shown in Figure 2E. The top view shows only the first atomic layer.

Table 3: Surface free energies in meV/Å^2 for the (2×2) CuCl(110) structures.

Structure	γ^{lean}	γ^{rich}
CuCl(110)	2.1	2.1
CuCl(110)-Cu	-4.0	-17.4
CuCl(110)-Cl	21.0	35.0

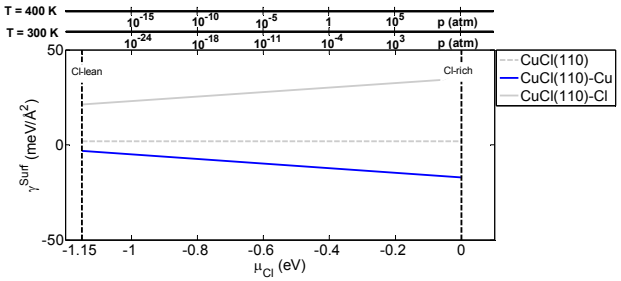

Figure 6: (Colored online) Surface free energy of the CuCl(110) surface structures listed in Table 3.

Table 4: Parameters of the reconstructed CuCl(110) ideal surface as defined in Figure 5.

	ω_1 (deg)	$\Delta_{1\perp}$(Å)	ω_2 (deg)	Cu_2-Cl_1(Å)	Cu_1-Cl_2(Å)
Unrelaxed	0.0	0.00	0.0	2.38	2.38
This Work	52.5	1.03	-2.0	2.28	2.34
Kahn *et al.*. [38]	41.2	0.68	0.0	2.17	2.23
Duke *et al.*. [34]	55.4	0.78	-5.5	2.31	2.37

3.2.3. *The CuCl(111) surface*

Results for the investigated CuCl(111) structures are presented in Table 5. Similar to the calculations carried out for the CuCl(100) surfaces, both Cu and Cl terminations have been considered, as well as structures with defects. The surface free energies for the various structures that we have considered are listed in Table 5 and shown as a function of the Cl chemical potential as well as *T* and *p* in Figure 7. The defected configuration CuCl(111):Cl-Cu appears to be the most stable over the whole Cl chemical potential range. The results in Figure7 show that the stability line of the CuCl(111):Cl-Cu structure follows the one of the CuCl(111):Cl surface, however, removing a Cu atom from the surface enhanced the stability of the system in the whole range of the Cl chemical potential. Figure 7 also illustrates that the discussed results applies for any values of *T* and *p*. As discussed earlier, however, for values greater than p~10^4 atm and T = 700 K, our calculations do not apply due to the phase transition in the CuCl crystal structure (see discussion in section 3.3).

With respect to the surface geometry, the Cl-terminated surface shows a 10% shortening of the Cu-Cl bond lengths at the surface and a 5% elongation of the bonds between the second and third layer atoms (see Figure 8 B). The Cu-terminated surface shows interesting behaviour with the Cl atoms in the second layer segregating to lie above the Cu atoms at the surface (Figure 8 A). Adding Cl atoms to the relaxed Cu-terminated surface, however, results in these segregated atoms returning to their original positions. It is worth mentioning that Wang and co-workers [39] have used the Cu-terminated (111) structures to investigate many adsorption systems, however, they have not considered the segregation behaviour for this surface.

Table 5: Surface free energies in meV/Å^2 for the (2×2) CuCl(111) structures.

Structure	γ^{lean}	γ^{rich}
CuCl(111):Cu	101.7	145.5
CuCl(111):Cu-Cu	36.1	58.0
CuCl(111):Cu-Cl	42.0	107.7
CuCl(111):Cl	19.4	-24.4
CuCl(111):Cl-Cl	22.2	0.3
CuCl(111):Cl-Cu	16.2	-49.5

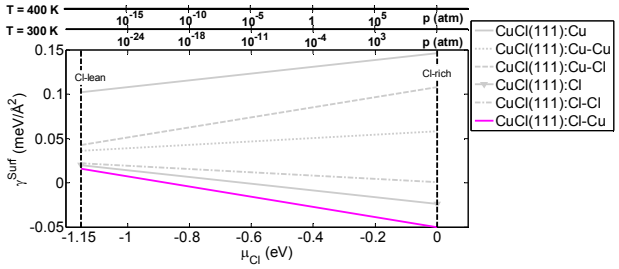

Figure 7: (Colored online) Surface free energy of the CuCl(111) surface structures listed in Table 5.

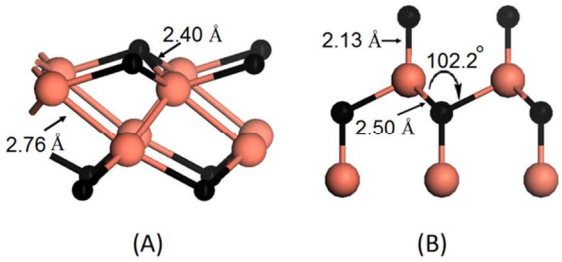

Figure 8: (Colored online) CuCl(111) structures: (A) the segregated CuCl(111):Cu surface and (B) the CuCl(111):Cl surface.

3.3. *CuCl crystal and the Wulff construction*

A theoretical prediction for the CuCl single crystal shape has been carried out by performing a Wulff construction utilizing the calculated surface free energies of the different CuCl structures. This is important as it identifies possible configurations of nano-particles under a range of conditions. Figure 9 (a) shows the surface free energies for the most stable CuCl configurations as a function of the chlorine chemical potential as well as real *T* and *p*. The structures of the most stable CuCl configurations are illustrated in Figure 10. Since the surface free energy of each configuration is a function of the chlorine chemical potential, the

resultant Wulff construction will vary within the proposed chlorine limits [see Figure 9 (b-e)].

Lorenz and Prener illustrated that at 407 °C (680 K), there is a transformation from the zinc-blende to a hexagonal wurtzite structure.[8] At high pressures (~10^4-10^5 atm), a phase transition of CuCl crystal has also been observed from the zinc-blende to rocksalt structure [4, 5, 9-11, 13, 40, 41]. We have chosen to investigate the stability of this system in the temperature and pressure range that produces only a zinc blende CuCl, namely 300 – 700 K.

Figure 9 (a) shows that in the range -1.15 < $\Delta\mu_{Cl}$ < -1.05, the CuCl(110)-Cu structure [see Figure 10 (A)] is the most stable configuration and makes the biggest contribution to the equilibrium shape of the crystal. The contributions of the (100) and (111) surfaces to the Wulff construction increase with an increase in the concentration of the chlorine environment. In the range -1.05 < $\Delta\mu_{Cl}$ < -0.47, the CuCl(100):Cl reconstructed surface [see Figure 10 (B)] makes the biggest contribution to the equilibrium shape [see Figure 9 (c)]. For $\Delta\mu_{Cl}$ > -0.47, the CuCl(111)Cl-Cu reconstructed surface [see Figure 10 (D)] is the most stable configuration and clearly constitutes the predominant plane in the equilibrium crystallite structure. This gives the crystal its semi-prism shape [see Figure 9 (d)]. Close to the chlorine rich-limit all of the crystal facets are built from the CuCl(111):Cl-Cu configuration [see Figure 9 (e)]. None of the other investigated structures contribute to the Wulff construction as their corresponding planes lie outside of the prism. This theoretical prediction is consistent with the shape of the CuCl nano-particles synthesised by Tomizuka *et al.* [11] and Xie *et al.*[1]. Tomizuka *et al.* [11] found that at temperature of 373-570 K and atmospheric pressure the CuCl crystals that were grown on the quartz tube formed the (111) polar surface. Xie *et al.* [1] found that under atmospheric pressure and maximum temperature of 415 K, the powder XRD data for different morphologies consist mainly of (111) and (110) facets with different ratios depending on the shape of the crystal. However, those with more (111) facets exhibited greater reactivity.

It should also be noted that at T = 300 and 400 K a phase transition of the CuCl crystal from zinc-blende to rocksalt is expected to take place at $\Delta\mu_{Cl}$ ~ -0.17 and ~-0.26 eV, respectively ($p \sim 10^4$ atm). Beyond these values, as represented by the shaded area in Figure 9(a), it is anticipated that our calculations may not be relevant due to a change in crystal structure. At T = 700 K, our calculations also aren't expected to apply for the whole range of $\Delta\mu_{Cl}$ as the CuCl crystal will at some point either be transformed from the zinc-blende to hexagonal wurtzite structure, or melted.

Cite this: DOI:

www.rsc.org/xxxxxx

Paper

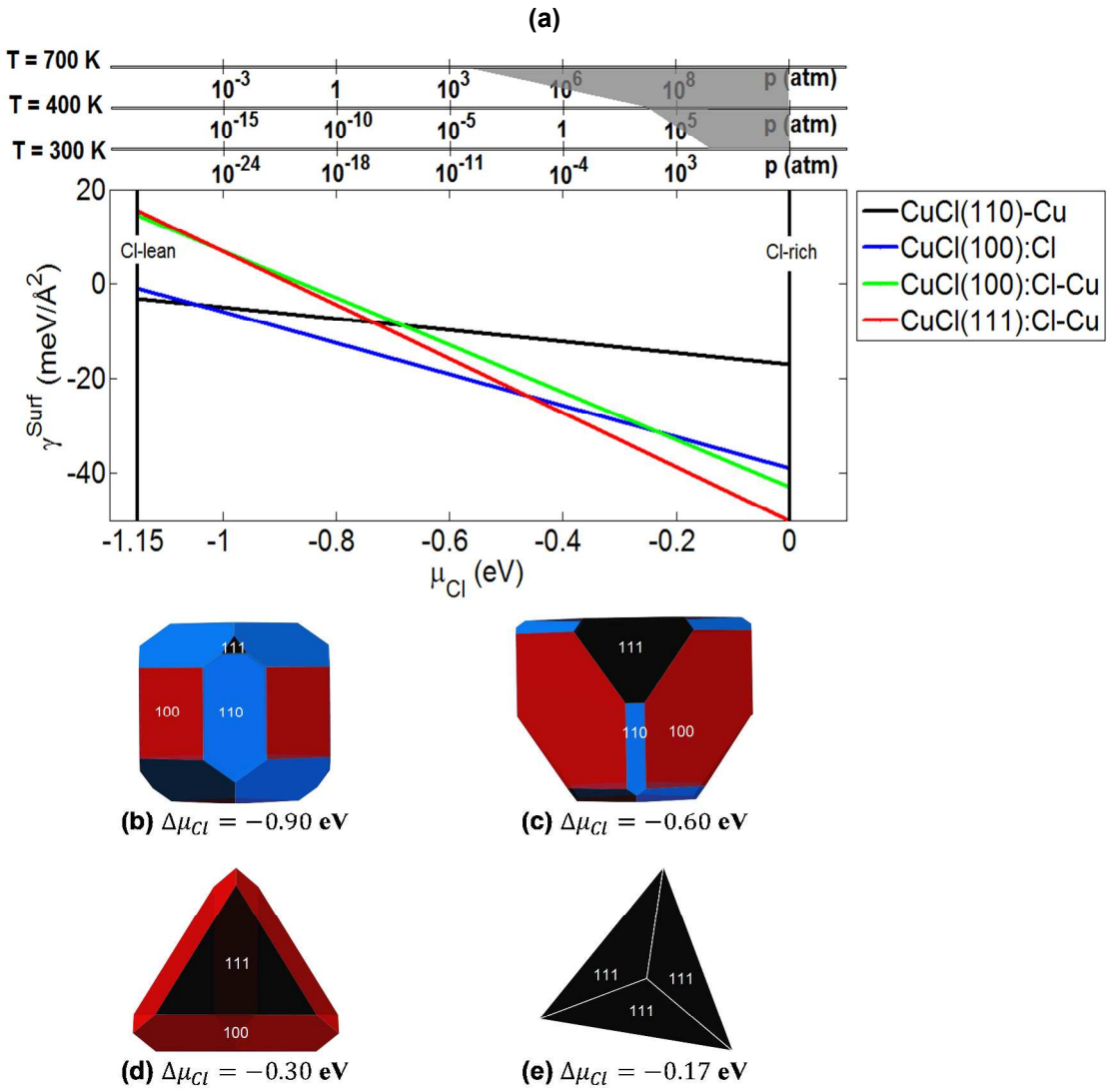

Figure 9: (Colored online) (a) Surface free energies of the lowest energy structures among the CuCl(100), CuCl(111) and CuCl(110) configurations. The shaded area indicates the range of *T* and *p* over which our calculations may not be relevant due to a structural phase transition (see the text for details). (b-e) Wulff constructions of the CuCl crystal for different $\Delta\mu_{Cl}$.

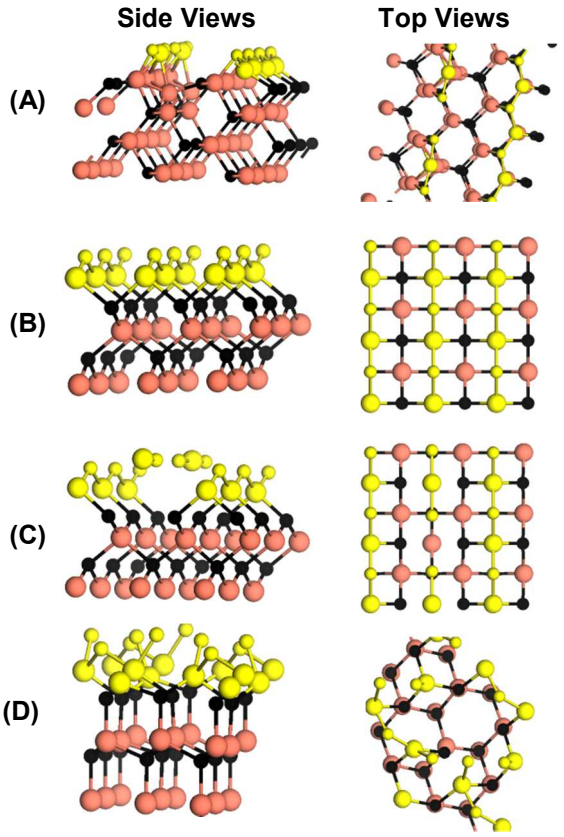

Figure 10: (Colored online) Side and top views of the most stable CuCl structures presented in Figure 9. (A) CuCl(110)-Cu, (B) CuCl(100):Cl, (C) CuCl(100):Cl-Cu, and (D) CuCl(111):Cl-Cu. Balls in yellow denote atoms in the first and second layers.

4. Conclusions

We have studied the structures of the low index surfaces of zinc-blende CuCl by performing first-principle density functional calculations. It was found that the Cl-terminated (100) and (111) configurations exhibit a small relaxation in the Cu-Cl bond at the surface. We also found for the Cu-terminated (111) surface that the Cl atoms segregate to lie above the Cu atoms at the surface.

The total free energies obtained by DFT have also been combined with *ab initio* atomistic thermodynamics to calculate the surface free energy for various surface terminations as a function of the chlorine chemical potential. This has enabled us to show that the CuCl(110)-Cu defected surface is the most stable configuration under Cl-lean conditions. Under Cl-rich conditions, on the other hand, the CuCl(111):Cl-Cu defected surface is the most stable, and hence contributes the most to the Wulff construction. This results in a prism shape in agreement with the experimental findings. The enhanced stability of the defected structures may arise from the removal of surface atoms providing more freedom for the remaining atoms to minimise the overall energy of the system.

Acknowledgement

This research was undertaken on the NCI National Facility in Canberra, Australia, which is supported by the Australian Commonwealth Government. Computational resources used in this work were also provided by Intersect Australia Ltd. I.A.S. acknowledges the support of the Deanship of Scientific Research at Taibah University-Saudi Arabia. M.W.R., J.C.M., E.M.K. and B.Z.D. acknowledge the Australian Research Council (ARC) for support (Project no. DP0988907). MWR also acknowledges the Polish Ministry of Science and Higher Education for support (Project no 06/62/DSPB/214/2015).

Notes and references

[a] *Taibah University, College of Engineering at Yanbu, Yanbu 41911, Saudi Arabia. Fax: (+966) 14 390 1483; Tel: (+966) 538 036 943; E-mail: isuleman@taibahu.edu.sa, ellariest@gmail.com*

[b] *The University of Newcastle, School of Mathematical and Physical Sciences, Newcastle 2308 NSW, Australia.*

[c] *The University of Newcastle, School of Engineering, Newcastle 2308 NSW, Australia.*

[d] *Murdoch University School of Engineering and Information Technology, Perth 6150 WA, Australia.*

[†] *Also at the Institute of Physics, Poznan University of Technology, 62-956 Poznan, Poland*

[††] *Also at School of Chemistry, The University of Sydney, NSW, Australia*

1. T. Xie, M. Gong, Z.-Q. Niu, S.-A. Li, X.-Y. Yan and Y.-D. Li, *Nano Res.*, 2010, **3**, 174-179.
2. J. Wang, C. Xu and G. Lv, *Appl. Surf. Sci.*, 2006, **252**, 6294-6303.
3. B. Amrani, T. Benmessabih, M. Tahiri, I. Chiboub, S. Hiadsi and F. Hamdache, *Physica B: Condensed Matter (Amsterdam, Netherlands)*, 2006, **381**, 179-186.
4. S. Hull and D. A. Keen, *Physical Review B: Condensed Matter and Materials Physics*, 1994, **50**, 5868-5869.
5. J. Kvapil and B. Perner, *J. Cryst. Growth*, 1971, **8**, 162-164.
6. J. Liebertz, *Physica Status Solidi*, 1966, **15**, K123-K125.
7. C. T. Lin, E. Schoenherr, A. Schmeding, T. Ruf, A. Goebel and M. Cardona, *J. Cryst. Growth*, 1996, **167**, 612-615.
8. M. R. Lorenz and J. S. Prener, *Acta Crystallographica*, 1956, **9**, 538-539.
9. E. Rapoport and C. W. F. T. Pistorius, *Physical Review*, 1968, **172**, 838-847.
10. N. R. Serebryanaya, S. V. Popova and A. P. Rusakov, *Fizika Tverdogo Tela (Sankt-Peterburg)*, 1975, **17**, 2772-2774.
11. A. Tomizuka, H. Iwanaga and N. Shibata, *J. Cryst. Growth*, 1988, **91**, 27-32.
12. W. R. Wilcox and R. A. Corley, *Materials Research Bulletin*, 1967, **2**, 571-579.
13. R. W. G. Wyckoff and E. Ponsjak, *J. Am. Chem. Soc.*, 1922, **44**, 30-36.
14. G. Rousselet, P. Capdevienlle and M. Maumy, *Tetrahedron Lett.*, 1993, **34**, 6395-6398.
15. U. Patent, 165,802 (1875).
16. C. Y. Nakakura, V. M. Phanse and E. I. Altman, *Surf. Sci.*, 1997, **370**, L149-L157.
17. C. Y. Nakakura, G. Zheng and E. I. Altman, *Surf. Sci.*, 1998, **401**, 173-184.
18. M. Galeotti, B. Cortigiani, U. Bardi, B. V. Andryushechkin, A. N. Klimov and K. N. El'tsov, *J. Electron Spectrosc. Relat. Phenom.*, 1995, **76**, 91-96.
19. Q. Wang, G. Chen and J. Pei, *Journal of Alloys and Compounds*, 2013, **549**, 341-347.
20. B. Delley, *J. Chem. Phys.*, 1990, **92**, 508-517.
21. B. Delley, *J. Chem. Phys.*, 2000, **113**, 7756-7764.
22. J. P. Perdew, K. Burke and M. Ernzerhof, *Phys. Rev. Lett.* , 1996, **77**, 3865-3868.
23. J. P. Perdew, K. Burke and Y. Wang, *Phys. Rev. B: Condens. Matter* 1996, **54**, 16533-16539.
24. H. J. Monkhorst and J. D. Pack, *Phys. Rev. B*, 1976, **13**, 5188-5192.
25. G. Z. Wulff, *Kristallogr. Miner.*, 1901, **34**, 449.
26. W. Kaminsky, *J. Appl. Crystallogr.*, 2005, **38**, 566–567.
27. W. Kaminsky, *J. Appl. Crystallogr.*, 2007, **40**, 382–385.
28. J. Rogal, K. Reuter and M. Scheffler, *Phys.Rev. B: Condens. Matter Mater. Phys.*, 2007, **75**, 205433.
29. J. Rogal, K. Reuter and M. Scheffler, *Phys. Rev. Lett.*, 2007, **98**, 046101.
30. S. Peljhan and A. Kokalj, *J. Phys. Chem. C*, 2009, **113**, 14363 –14376.
31. C. Stampfl, A. Soon, S. Piccinin, H. Q. Shi and H. Zhang, *J. Phys.: Condens. Matter*, 2008, **20**, 184021.
32. M. W. Chase, Jr., *JANAF Thermochemical Tables*, 4th ed. edn., 1998.
33. D. F. Ramon, *CRC handbook of chemistry and physics: a ready-reference book of chemical and physical data*, 64th edn., 2000.
34. C. B. Duke, A. Paton, A. Lazarides and A. Kahn, *Phys. Rev. B: Condens. Matter*, 1996, **54**, 14692-14702.
35. M. H. Tsai, J. D. Dow, R. P. Wang and R. V. Kasowski, *Phys. Rev. B: Condens. Matter*, 1989, **40**, 9818-9823.
36. M. H. Tsai, W. M. Hu, J. D. Dow and O. F. Sankey, *J. Vac. Sci. Technol., A*, 1992, **10**, 2511-2514.
37. A. Soon, M. Todorova, B. Delley and C. Stampfl, *Phys. Rev. B*, 2007, **75**, 125420.
38. A. Kahn, S. Ahsan, W. Chen, M. Dumas, C. B. Duke and A. Paton, *Phys. Rev. Lett.*, 1992, **68**, 3200-3203.
39. X. Wang, W.-K. Chen and C.-H. Lu, *Appl. Surf. Sci.*, 2008, **254**, 4421-4431.
40. F. El Haj Hassan, A. Zaoui and W. Sekkal, *Materials Science & Engineering, B: Solid-State Materials for Advanced Technology*, 2001, **B87**, 40-47.
41. W. Sekkal, H. Aourag and M. Certier, *Journal of Physics and Chemistry of Solids*, 1998, **59**, 1293-1301.